A self-resonant plug-in IC antenna for DTT

A Self-Resonant Plug-In IC Antenna for DTT

D. Milanesio,[1, a)] G. Vecchi,[1] B. Baiocchi,[2] A. Cardinali,[3] S. Ceccuzzi,[3,4] D.L. Galindo Huertas,[1] D. Mascali,[5] G.S. Mauro,[5] F. Mirizzi,[4,6] A. Pidatella,[5] C. Ponti,[7] G.L. Ravera,[3] G. Torrisi,[5] and A.A. Tuccillo[4,6]

[1)] *Politecnico di Torino, Torino, Italy*
[2)] *CNR-ISTP, Milano, Italy*
[3)] *ENEA, Frascati, Italy*
[4)] *DTT S.C. a r.l., Frascati, Italy*
[5)] *INFN-LNS, Catania, Italy*
[6)] *Consorzio CREATE, Napoli, Italy*
[7)] *Roma Tre University, Rome, Italy*

[a)] *Corresponding author: daniele.milanesio@polito.it*

Abstract. Ion Cyclotron Range of Frequencies (ICRF) antennas are adopted in most of the existing nuclear fusion experiments. Their capability to couple high power to the plasma is known to be limited by a high input reflection coefficient and sometimes by high electric fields within the antenna box and immediately in front of it. In this work, we introduce a self-resonant IC strap antenna that can reach very good impedance matching, i.e. with very small power reflected back to the feeding lines; it is designed for the incoming Divertor Tokamak Test (DTT) experiment [1]. The antenna reaches matching for a bandwidth limited by the electrical size of the box, that is not compatible with operational planned frequency interval. Hence, we also propose an all-metal frequency structural tuning system; this allows launcher to be operated in frequency intervals of practical interest, e.g. from 60MHz to 90MHz. The overall antenna is a two-strap plug-in launcher that fits within DTT equatorial duct. After introducing the antenna concept, we describe a few optimization steps carried on through numerical codes, with a specific focus on the critical aspects mentioned above.

MOTIVATION AND BACKGROUND

Ion Cyclotron (IC) antennas are one of the most prominent auxiliary systems to deliver high power to the plasma in present-day experiments towards the realisation of controlled nuclear fusion with magnetic confinement. These antennas are installed and operated in almost all existing fusion experiments and they are envisioned for the next generation of tokamaks like ITER [2], SPARC [3], CFETR [4] and DEMO [5].

The working frequency, the required high power transferred to plasma, the limited available space and other mechanical and electromagnetic constrains limit the performance of IC antennas, which are usually characterized by very high reflection coefficients at their input ports. This reflects into high voltages along the input lines, which may cause potential damage to the system itself. The aim of this work is to introduce a self-resonant antenna concept; in particular, it may be operated on the DTT experiment from 60MHz to 90MHz without the drawbacks mentioned above. This paper provides a proof of principle and not a complete antenna design, being the mechanical, thermal and nuclear stresses not addressed at all. Please refer to [6] for a more detailed analysis of the IC system.

The organisation of this paper is as follows: first an overview of the self-resonant tunable concept is provided, afterwards the adopted tools and the implementation of this concept for DTT experiment are described.

INTRODUCTION TO TUNABLE RESONANT ANTENNAS

As well known, a (one port) structure is defined to be resonant if its input impedance $Z_{in}(f)$ is purely real at the reference frequency f_0, i.e. $\mathrm{Im}\{Z_{in}(f_0)\} = 0$, $Z_{in}(f_0) = R$. This remarkable property alone is not yet enough to make it practically usable; one also needs that the value of the real impedance at the resonance frequency matches the desired value set by generators and feeding line, R_0; the latter in typical IC systems is of the order of a few tens of Ohms.

In typical ICRH systems, this necessary resonance property achieves after the tuning and matching system (TMS) located outside the vacuum chamber, as the antenna alone cannot reach this condition. A self-resonant antenna, on the contrary, is characterized by this property at its own port, thus relaxing the task of the TMS or dispensing of it altogether.

It is also well known that the (self) resonance of antennas happens when the electrical length is comparable to the wavelength; in a first approximation, we can employ here the vacuum wavelength $\lambda \approx \lambda_0 = c/f$ (the impact of plasma is minor on these considerations). Using conventional types of antenna, like the ubiquitous strap topology, requires that the length L of the antenna be $L \approx \lambda/2$, and that requires sizes typically not available in most machines, including DTT. A less known fact is that however the very first resonance happens at $L \approx \lambda/4$ for some antenna topologies.

For compatibility with the ICRH antenna environment, we will exclude non metal components, and variable capacitors even outside the vacuum chamber. With these constraints, the quarter-wavelength (QW) resonance that appears of most interests here is based on the "L-type" antenna depicted in Figure 1.a, with $L_L \approx \lambda/4$ (its name refers to its resemblance to the L letter).

The working principle can be understood in terms of transmission lines: the L is terminated on an open, and neglecting material and radiation losses at the QW resonance one expects $Z_{in} \to 0$ (open to short); considering (small) radiation losses (plasma loading), one then expects to have a (very) small impedance for the "L" antenna. In practice, this must be augmented by a structure that allows to bring its resonance impedance to a practical value; the typical impedance matching structure, is depicted in Figure 1.b, and is typically called the inverted-F antenna (IFA); as for the "L" name, this derives from the resemblance to the "F" letter. The arrow included in Figure 1.b indicates that the insertion point is a design parameters to be selected.

It is a general fact that small resonant antennas are narrow-band. The typical required operational bandwidth of ICRH system is in the order of 2:1 (e.g., in DTT from 60 to 90 MHz); as a result, a resonant antenna need to be also complemented by a *structural* tuning mechanism.

The envisioned frequency tuning mechanism is schematically depicted in Figure 1.c. It is based on the principle of changing the per-unit-length capacitance of the transmission line; this does not impact the phase velocity (in the absence of dielectrics it is always the light velocity, c), but it impacts on the characteristic impedance, and hence (for a given radiation loading) on the (complex) input impedance; as the impedance matching structure is not changed, this way the inductance-to-capacitance resonance balance happens at different frequencies.

An important issue in ICRH antennas is power handling in terms of maximum electric field; this topic will be properly addressed in future communications.

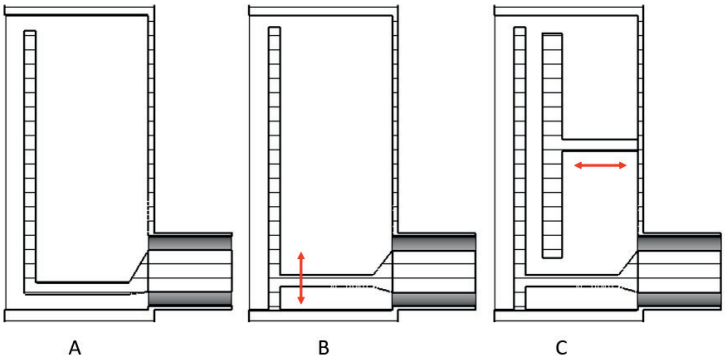

FIGURE 1. Poloidal cut of the resonant antenna (Faraday Screen omitted). a): conceptual "L" antenna; b): "L" antenna with impedance matching ("IFA"); c) IFA antenna with proposed frequency tuning. Arrows indicate geometrical variability; the impedance matching in b) is structural, optimized at design and unchanged during operation; the frequency tuning in c) is movable to match the frequency of operation.

ANALYSIS AND SELECTION OF A TUNABLE RESONANT IC LAUNCHER FOR THE DTT EXPERIMENT

Adopted tools and simulations setup

Figure 2 depicts the setup adopted in CST-MWS to investigate among the available geometrical options and then to select the most promising launcher for further optimization. An "equivalent" plasma loading was tailored for this purpose, using as a reference the analysis performed with TOPICA code on a preliminary antenna geometry designed

for the DTT experiment (see [1] for further details). To be more specific, a user-defined lossy dielectric ($\varepsilon_r = 225$ and $tan\delta = 1.17$ at 90MHz) located in front of the antenna mouth, right after a small vacuum layer, produced the same coupling as the above mentioned TOPICA simulations. The authors are therefore aware that this an arbitrary pick and a different loading may lead to slightly different conclusions.

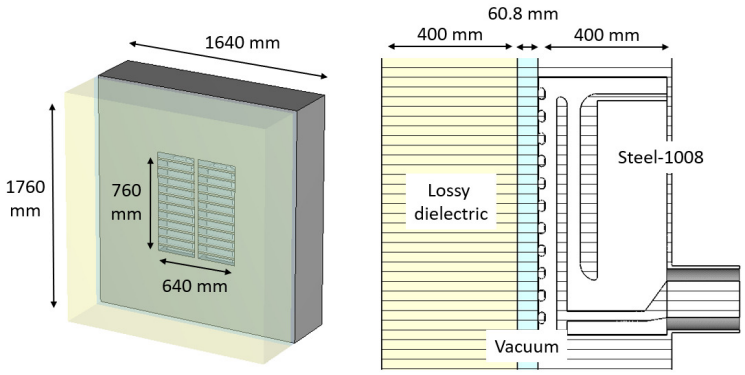

FIGURE 2. Front view (left) and poloidal cut (right) of the setup adopted in CST-MWS with some relevant dimensions (in millimeters). The two-strap antenna is enclosed within a box (all metallic elements are assumed to be Steel-1008) and located in front of a 60.8mm vacuum layer followed by a 400mm lossy dielectric.

Simulated geometries

The aim of this section is to present an extensive set of candidate geometries for the DTT experiment, keeping in mind that the resonant antenna is to be able to be operated throughout the entire IC frequency range, i.e. from 60MHz to 90MHz. As mentioned in the introduction, this flexibility is guaranteed by the presence of a tuning element (TE) that can be radially shifted, allowing to move the antenna resonance in frequency.

Since the size of the antenna box is basically constrained by the size of DTT equatorial duct, we focused our attention on the strap and TE geometry selection. Figures 3 and 4 document the most relevant geometries tested in CST-MWS. It should be mentioned that, even though all combinations were simulated, for sake of simplicity Figure 3 reports only the simplest TE with an asymmetric pole (labelled as TE2 in Figure 4), which was eventually chosen. It is worth mentioning that also the Faraday Screen (FS) was optimized during the process, even though we observed a negligible impact on the resonance position. We therefore adopted a classical 50% transparency factor and rounded bars with a section of about 25mm in order to allow cooling.

The strap geometry is characterized by a radial lofted feeder that connects the coaxial cable inner conductor to the radiating part of the strap itself. Within this last element, one can identify two extremities that can be closed either with an open circuit or with a short; all possible combinations were tested. We started with an open/open solution (S1) leading to the above mentioned "L" antenna. We then closed one end with a short circuit, that could be located in the antenna front part (as in S2a, S3a and S3b) or in the back wall (S2b). A few more peculiar solutions (S5, S6a, S6b and S6c) were also tested to investigate the effect of the short position on the input reflection coefficient. We eventually closed also the second end with a short, again connected both in the front (S4a) or in the back (S4b). To conclude, a passive strap coupled to a loop was also included in the pool of candidates.

The second element to be analysed was the TE, as described in Figure 4. We started with a symmetric TE (TE1) and we afterwards translated the moving pole to one side (TE2), testing also all intermediate positions. The next set of TEs was characterized by a folded structure, that could be connected to the back wall once (TE3, TE5 and TE6) or twice (TE4). Eventually a double TE was simulated (TE7), both considering the two elements as independently moving and keeping constant their relative distance.

Since the driving requirement about frequency flexibility can be reached by radially shifting the TE itself, it was immediately evident that a folded or a double TE considerably reduced the available radial movement, hence they had to be dropped. Similarly, only S3a and S4a allowed the presence of a resonance throughout the complete frequency range, while all other strap geometries were discarded. It is nevertheless important to stress that for reduced frequency

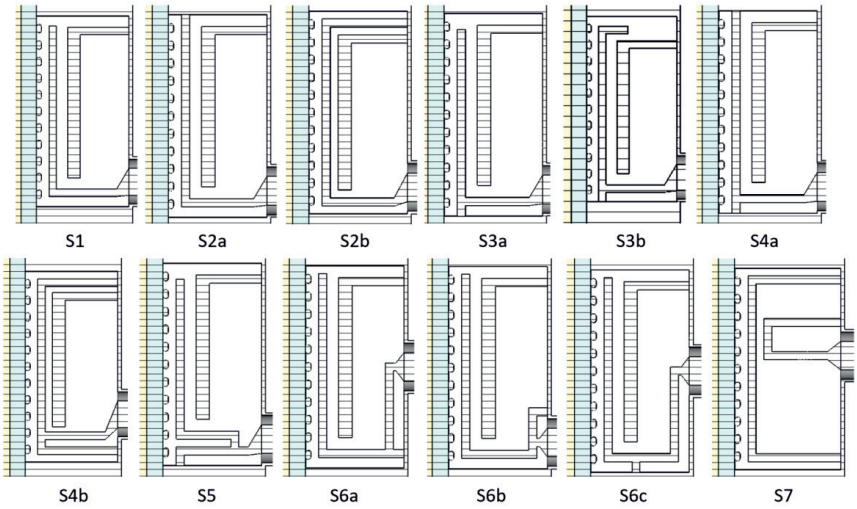

FIGURE 3. Tested solutions in terms of antenna strap shape.

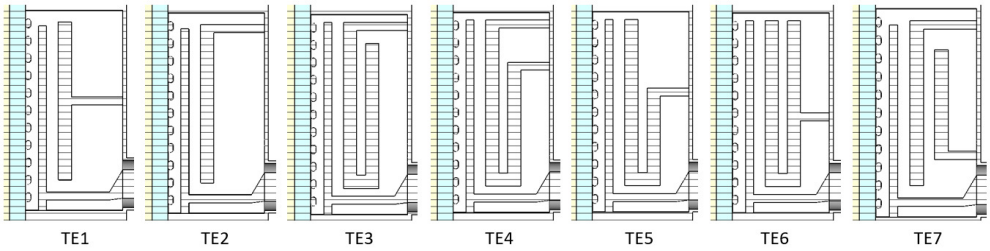

FIGURE 4. Tested solutions in terms of tuning elements.

bandwidth applications (or even better for a single working frequency antenna), some of the discarded solutions may be perfectly working.

Simulation results

Figures 5, 6 and 7 document the frequency behaviour of the S_{11} magnitude for geometries S3aTE1, S3aTE2 and S4aTE1 respectively. In all cases a 4.5cm distance between the strap and the TE was assumed, corresponding to a 22cm radial extension of the TE.

To comment further, S3aTE1 covers from about 65MHz to about 80MHz through the TE radial movement, while a second resonance is observed around 84MHz (and it is only slightly influenced by the TE movement). Frequencies below 65MHz can be reached by reducing the strap-TE distance, which will lead to a local electric field increase in that region; on the contrary, frequencies above 85MHz cannot be accessed. A similar behavior in frequency can be observed for S3aTE2 for what concerns the tunable resonance; the second resonance covers instead the upper frequency range up to 90MHz. S4aTE1 can cover the entire frequency interval, even though the S_{11} magnitude decreases to only about -4dB at 91.84MHz.

Figure 8 reports the electric field magnitude for the three geometries under study at the shown lower resonance, given an incident power of 800kW. To be more specific, S3aTE1 model was tested at 65.84MHz, where a -23.7dB S_{11} magnitude allowed to couple 797kW of power, S3aTE2 was tested at 59.92MHz (S_{11}=-12.5dB, $P_{coupled}$=755kW) while S4aTE1 at 59.44MHz (S_{11}=-18.4dB, $P_{coupled}$=771kW).

In general, S3aTE1 shows field maxima that are a bit lower than S3aTE2, but they are evaluated at higher frequency. S4aTE1 is without doubt the worst geometry in terms of local electric fields, which are extremely high around the TE. By looking at both the frequency behaviour and the local electric field maxima, the most promising geometry

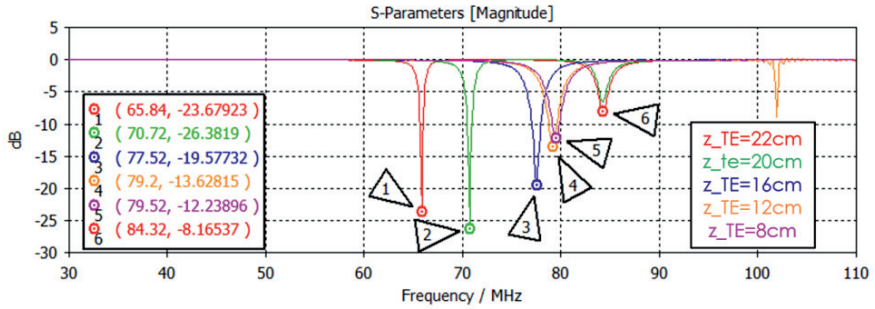

FIGURE 5. S11 magnitude (in dB) for geometry S3aTE1 as a function of the radial position of the TE (22cm corresponds to a minimum gap of 4.5cm between the strap and the TE).

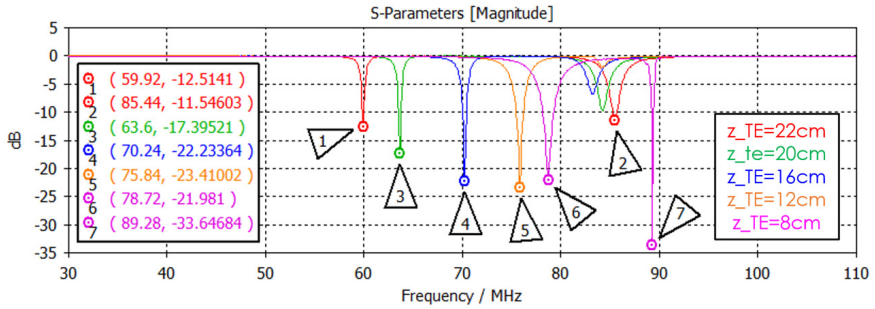

FIGURE 6. S11 magnitude (in dB) for geometry S3aTE2 as a function of the radial position of the TE (22cm corresponds to a minimum gap of 4.5cm between the strap and the TE).

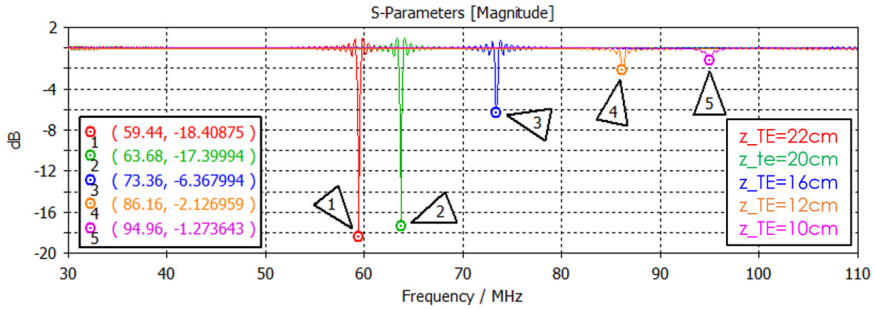

FIGURE 7. S11 magnitude (in dB) for geometry S4aTE1 as a function of the radial position of the TE (22cm corresponds to a minimum gap of 4.5cm between the strap and the TE).

is S3TE2. Its geometrical optimization and the behaviour at different frequencies and loadings will be described in future communications.

CONCLUSION AND FUTURE WORK

This paper presented a full metal tunable self-resonant antenna concept that can be applied to DTT experiment. Several geometrical solutions were tested and a promising candidate was selected; the proposed launcher can be tuned to resonate from 60MHz to 90MHz, guaranteeing a low input reflection coefficient throughout the entire frequency bandwidth. A first estimate of the local electric fields within the antenna box indicated that a further geometrical optimization is required to successfully operate the antenna.

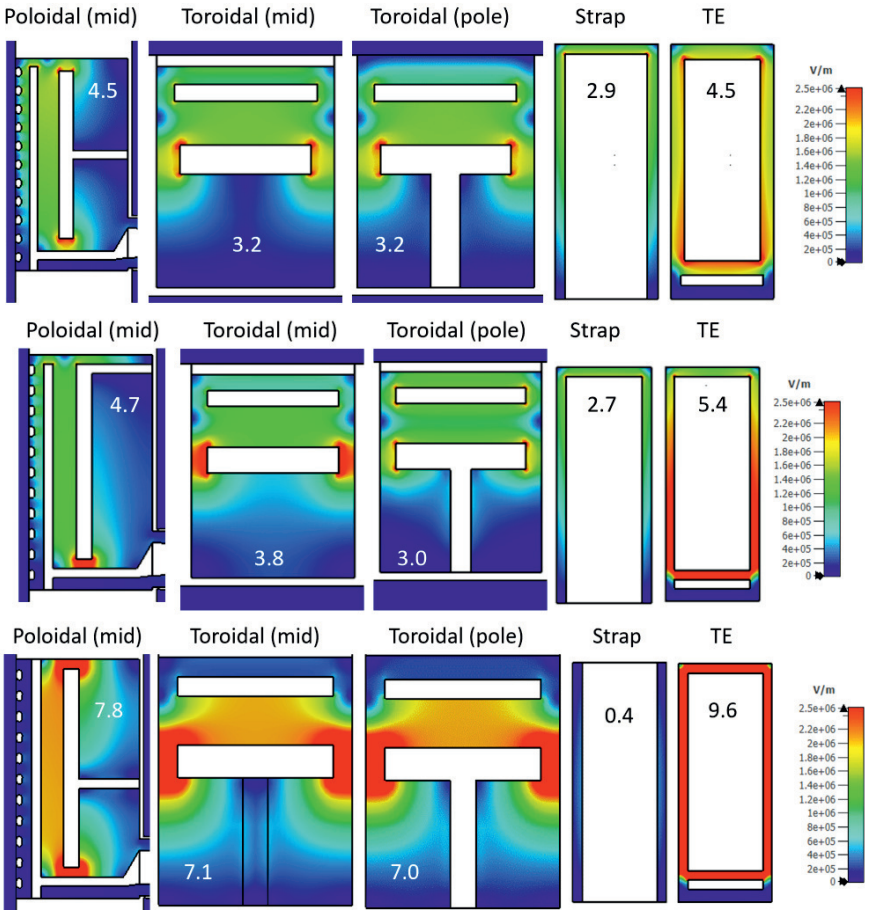

FIGURE 8. Magnitude of the max electric field (clamped to 2.5MV/m) evaluated with CST-MWS for different antenna geometries and sections, given 800kW of incident power at the lower available resonance. From top to bottom, geometries S3aTE1, S3aTE2 and S4aTE2 are shown. From left to right, the fields are plotted at the poloidal mid section, at the toroidal mid section, at the toroidal position of the TE pole, at the radial mid section of the strap, at the radial mid section of the TE. The maximum electric field for each section (as indicated by CST-MWS) is also reported on the picture, expressed in MV/m.

REFERENCES

1. R. Martone, R. Albanese, F. Crisanti, P. Martin, and A. Pizzuto, "Divertor tokamak test facility: Interim design report," Tech. Rep. 978-88-8286-378-4 (2019).
2. W. Helou and et Al., To be submitted to Nuclear Fusion (2022).
3. Y. Lin, J. C. Wright, and S. J. Wukitch, "Physics basis for the icrf system of the sparc tokamak," Journal of Plasma Physics **86**, 865860506 (2020).
4. Y. Wan, J. Li, Y. Liu, X. Wang, V. Chan, C. Chen, X. Duan, P. Fu, X. Gao, K. Feng, S. Liu, Y. Song, P. Weng, B. Wan, F. Wan, H. Wang, S. Wu, M. Ye, Q. Yang, G. Zheng, G. Zhuang, and Q. Li, "Overview of the present progress and activities on the CFETR," Nuclear Fusion **57**, 102009 (2017).
5. M. Tran, P. Agostinetti, G. Aiello, K. Avramidis, B. Baiocchi, M. Barbisan, V. Bobkov, S. Briefi, A. Bruschi, R. Chavan, I. Chelis, C. Day, R. Delogu, B. Ell, F. Fanale, A. Fassina, U. Fantz, H. Faugel, L. Figini, D. Fiorucci, R. Friedl, T. Franke, G. Gantenbein, S. Garavaglia, G. Granucci, S. Hanke, J.-P. Hogge, C. Hopf, A. Kostic, S. Illy, Z. Ioannidis, J. Jelonnek, J. Jin, G. Latsas, F. Louche, V. Maquet, R. Maggiora, A. Messiaen, D. Milanesio, A. Mimo, A. Moro, R. Ochoukov, J. Ongena, I. Pagonakis, D. Peponis, A. Pimazzoni, R. Ragona, N. Rispoli, T. Ruess, T. Rzesnicki, T. Scherer, P. Spaeh, G. Starnella, D. Strauss, M. Thumm, W. Tierens, I. Tigelis, C. Tsironis, M. Usoltceva, D. Van Eester, F. Veronese, P. Vincenzi, F. Wagner, C. Wu, F. Zeus, and W. Zhang, "Status and future development of heating and current drive for the EU DEMO," Fusion Engineering and Design **180**, 113159 (2022).
6. S. Ceccuzzi, B. Baiocchi, A. Cardinali, G. D. Gironimo, G. Granucci, D. Liuzza, D. Mascali, G. Mauro, D. Milanesio, F. Mirizzi, A. Pidatella, S. Piras, C. Ponti, G. Ravera, G. Schettini, G. Torrisi, A. Tuccillo, and G. Vecchi, "The ICRF antenna of DTT: Design status and perspectives," in *Proceedings of the 24th Topical Conference on Radio-frequency Power in Plasma* (2022).